

02-D Magnetohydrodynamics Boundary Layer Flow of Cu-Ag-TiO₃-Al₂O₃-H₂O-C₂H₆O₂ Mixtures: Explicit Numerical and Stability Approach

M. Ferdows^{1,2,*}, D. Liu^{1,*} and B. R. Ramachandran¹

¹College of Engineering and Science, Louisiana Tech University, Ruston, 71270, USA

²Department of Applied Mathematics, University of Dhaka, Dhaka 1000, Bangladesh

Abstract: An analysis is present for an unsteady, viscous incompressible flow with four types of nanoparticles, namely (Cu, Ag, Al₂O₃, TiO₃). It also considers water and Ethylene Glycol (C₂H₆O₂, EG) as base fluids which are electrically conducting in the presence of a transverse magnetic field. The transformed nonlinear governing equations which are non-similar are solved with suitable transformations and a robust explicit finite difference method. The controlling flow characteristic parameters such as Prandtl number (Pr), Magnetic parameter (M), Richardson number (Ri), Reynolds number (Re) and volume fraction of nanofluids (ϕ) are discussed for dimensionless velocity and temperature flow profiles. Stability and convergence of the derived solutions are considered. It is observed that in the momentum profiles, the magnetic field has a great impact on Reynolds number. Richardson number has a significant impact in the momentum boundary layer thickness. The effect of different nanoparticles with different base fluids is analyzed and compared between steady and non-steady states. Shear stress and Nusselt number are also discussed for different parameters. This study has applications in propulsion system and magnetic nanomaterials processing.

Keywords: Magnetohydrodynamics, nanoparticles, steady-unsteady state condition, explicit finite difference, stability analysis.

1. INTRODUCTION

Natural convective heat transfer has wide application in electronic cooling, heat exchanges, double pane windows, fusion reactors, dispersion of metals, metallurgy, design of magneto hydrodynamic (MHD) pumps, MHD generators and MHD flow meters etc. MHD convection problems have many application in fields of stellar and planetary magnetospheres, aeronautics and chemical and electrical Engineering. These problems are very significant in Medicine and Biology [1] as well.

Enhancement of heat transfer is important from an energy savings perspective. Fluids like water and oil have low thermal conductivity and so they are limited in their heat transfer abilities especially as the systems are miniaturized. Use of nanoparticles together with fluids result in higher conductivity. Usually the enhanced thermal conductivity nanoparticulate fluids is accompanied by minimal clogging in flow passages, long term stability, agglomeration, and homogeneity. However, these properties are dependent on the size of solid particles and behavior of different nanoparticles. Several authors have investigated the significant effects of nanoparticles with different base fluid and analyzed the magnetic field effect. Hellums

and Churchill [2] solved unsteady natural convection flow using an explicit finite difference method. Soundalgekar and Ganesan [3] analyzed a transient free convection flow using implicit method. Remeli *et al.*, analyzed the effect of steady Marangoni boundary layer flow with three different types of nanoparticles, Cu, Al₂O₃ and TiO₂ [4]. The steady two-dimensional Falkner–Skan boundary layer flow with similar solutions for four different types of nanoparticles, (Cu), (Al₂O₃), (TiO₂) and (Ag) together with two different types of the base fluids, namely, water and ethylene glycol, was analyzed by the Ferdows [5]. Historically, a uniform transverse magnetic field is used to control electrically conducting fluids. Free convection effects combined with magnetic field on stokes problem have been investigated by Rossow [6] and Soundalgekar *et al.* [7]. The effect of heat and mass transfer on MHD and buoyancy force in a magnetic field were examined by Elbashbeshy [8]. A numerical solution of unsteady MHD flow past a semi infinite isothermal vertical plate was obtained by Ganesan and Palani [9]. In the presence of magneto and thermal radiation effects, a mixed convection heat transfer pasta permeable vertical plate was analyzed by Aydin and Kaya [10]. Unsteady MHD mixed convective boundary layer flow of a nanofluid were studied by the Ferdows using finite difference method [11] in which they used Brownian motion to incorporate nanofluid instead of nanoparticles. A study has also been made of an electrically conducting fluid past a

*Address correspondence to this author at the College of Engineering and Science, Louisiana Tech University, Ruston, 71270, USA; Tel: +1 318 308 6157; E-mails: ferdows@du.ac.bd, donliu@latech.edu

stretching plate and the effect of magnetic parameter [12]. An MHD boundary layer flow of nanofluid of power law flow over a surface has been observed [13] in the presence of transverse magnetic field and found the effects of nanofluid Brownian motion. More investigations of flow and heat transfer in a different geometry filled with several nanoparticles and its application were studied by multiple investigators [14-17].

Until now the stability and convergence characteristics of nanoparticles flow of the boundary layer have been ignored by most studies. So, in this paper our aim is to investigate the effects of physical parameters in time dependent two dimensional flow of boundary layer nanofluid particles with the influence of magnetic media considering stability and convergence analysis. Explicit finite difference method [18] has been used to solve the partial differential equations with stability and convergence analysis to solve the obtained non-similar equations. An extensive development for finite difference solution with high order has been discussed for modeling of fluid flow equations for instant [19, 20]. We propose a time-space approach for simulations of the coupled nonlinear ordinary governing equations.

2. MATHEMATICAL MODEL OF FLOW

Here we assume the vertical wall at $Y = 0$. The boundary wall is kept at constant but different temperature and Y is the coordinate measured normal to the adiabatic. The physical configuration and coordinate system is shown in Figure 1.

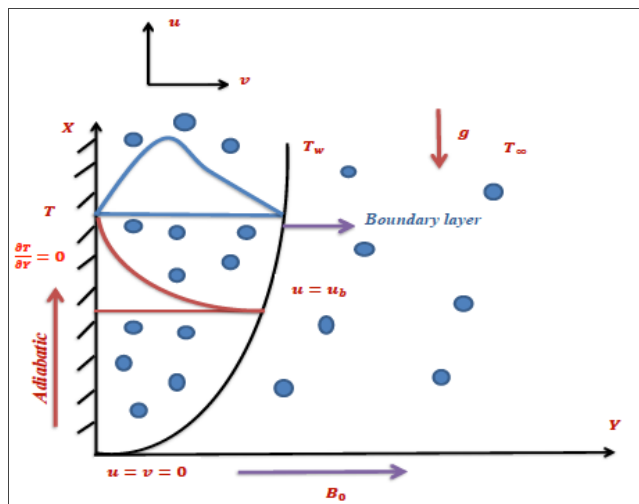


Figure 1: Physical and coordinate model.

Water is taken to be the base nanofluid. Wall temperature is T_w and velocity is $u = v = 0$. A uniform magnetic field B_0 is imposed normal to the plate. The magnetic induction vector B_0 can be taken as $B = (0, B_0, 0)$. Under the usual boundary layer approximation, the MHD time dependent nanofluid flow and heat transfer are governed by the following equations;

The continuity equation:

$$\frac{\partial u}{\partial x} + \frac{\partial v}{\partial y} = 0 \quad (1)$$

Momentum equation:

$$\rho_{nf} \left(\frac{\partial u}{\partial t} + u \frac{\partial u}{\partial x} + v \frac{\partial u}{\partial y} \right) = \mu_{nf} \frac{\partial^2 u}{\partial y^2} \pm g(T - T_{\infty})(\rho\beta)_{nf} - \sigma\beta_0^2 u \quad (2)$$

Energy equation:

$$\frac{\partial T}{\partial t} + u \frac{\partial T}{\partial x} + v \frac{\partial T}{\partial y} = \alpha_{nf} \frac{\partial^2 T}{\partial y^2} \quad (3)$$

Boundary condition: $u=v=0, T=T_w, y=0$

$$u=u_b, v=0, T=T_{\infty}, y \rightarrow \infty \quad (4)$$

Here the parameters are;

$$\rho_{nf} = (1 - \phi)\rho_f + \phi\rho_s \text{ is the density,}$$

$$(\rho c_p)_{nf} = (1 - \phi)(\rho c_p)_f + \phi(\rho c_p)_s \text{ is the heat capacitance,}$$

$$(\beta)_{nf} = (1 - \phi)(\beta)_f + \phi(\beta)_s \text{ is the thermal expansion coefficient,}$$

$$k_{nf} = k_f \frac{k_s + 2k_f - 2\phi(k_f - k_s)}{k_s + 2k_f + 2\phi(k - k_s)} \text{ is the thermal conductivity of the nanofluid,}$$

$$\alpha_{nf} = \frac{k_{nf}}{(\rho c_p)_{nf}} \text{ is the thermal diffusivity,}$$

$$\mu_{nf} = \frac{\mu_f}{(1 - \phi)^{2.5}} \text{ is dynamic viscosity,}$$

$$Pr = \frac{\mu_f}{\alpha_f} \text{ is Prandtl number.}$$

The above equations have dimensional variables are transformed to dimensionless variables by using the following dimensionless dependent and independent variables;

$$X = \frac{x}{L}, Y = \frac{y}{L}, U = \frac{u}{u_b}, V = \frac{v}{u_b},$$

$$\bar{T} = \theta = \frac{T - T_\infty}{T_w - T_\infty}, \tau = \frac{t u_b}{L} \quad (5)$$

Using the above variables into Eqs. (1)-(3), we find the following non dimensional equations as;

$$\frac{\partial U}{\partial X} + \frac{\partial V}{\partial Y} = 0 \quad (6)$$

$$\frac{\partial U}{\partial \tau} + U \frac{\partial U}{\partial X} + V \frac{\partial U}{\partial Y} = \frac{\rho_f}{\text{Re}(1-\phi)^{2.5} \{ (1-\phi)\rho_f + \phi\rho_s \}}$$

$$\frac{\partial^2 U}{\partial Y^2} \pm \frac{R_f}{\beta_f} \frac{(1-\phi)(\rho\beta)_f + \phi(\rho\beta)_s}{(1-\phi)\rho_f + \phi\rho_s} \bar{T} - \frac{UM\rho_f}{(1-\phi)\rho_f + \phi\rho_s}$$

$$\frac{\partial \bar{T}}{\partial \tau} + U \frac{\partial \bar{T}}{\partial X} + V \frac{\partial \bar{T}}{\partial Y} = \frac{k_{nf}/k_f}{\left[1 - \phi + \phi \frac{(\rho c_p)_s}{(\rho c_p)_f} \right] \text{Pr Re}} \frac{\partial^2 \bar{T}}{\partial Y^2} \quad (8)$$

And therefore the corresponding boundary conditions take the following form;

$$\tau \leq 0, U = 0, V = 0, \bar{T} = 0 \quad \text{everywhere}$$

$$\tau \leq 0, U = 0, V = 0, \bar{T} = 0 \quad \text{at } X = 0 \quad (9)$$

$$U = 0, V = 0, \bar{T} = 1 \quad \text{at } Y = 0$$

$$U = 1, V = 0, \bar{T} = 0 \quad \text{at } Y = \infty$$

where, Magnetic parameter, $M = \frac{\sigma \beta_0^2 L}{\rho_f u_b}$,

Local Reynolds number, $\text{Re} = \frac{v_b L}{\nu_f}$,

Richardson number, $Ri = \frac{g \beta_f (T_w - T_\infty) L}{u_b^2} = Gr / \text{Re}^2$,

Grashof number, $Gr = \frac{g \beta_f (T_w - T_\infty) L^3}{\nu_f^2}$,

Nusselt number, $\text{Nu} = \frac{hL}{K_f}$,

The heat transfer coefficient is expressed as;

$$h = \frac{q_w}{T_w - T_\infty} \quad (10)$$

The thermal conductivity is expressed as;

$$K_{nf} = \frac{q_w}{k_f} \frac{\partial T}{\partial y} \quad (11)$$

$$K_{nf} = k_f \frac{k_s + 2k_f - 2\phi(k_f - k_s)}{k_s + 2k_f + 2\phi(k_f - k_s)} \quad (12)$$

Using (10), (11), (12) we have;

$$\text{Nu} = -\frac{K_{nf}}{K_f} \theta'(0)$$

Skink friction coefficient, $C_f = \frac{\mu_{nf}}{\rho_f u_b^2} \left(\frac{\partial u}{\partial y} \right)_{y=0}$

$$\Rightarrow C_f \text{Re} = \frac{1}{(1-\phi)^{2.5}} \left(\frac{\partial U}{\partial Y} \right)_{Y=0}$$

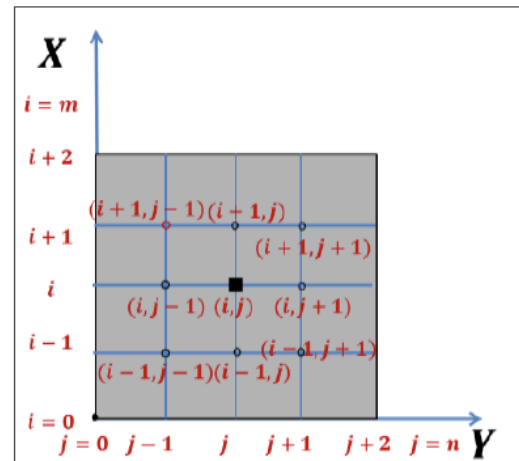
3. NUMERICAL PROCEDURE

In order to solve the non-similar unsteady coupled non-linear partial differential equations, the explicit finite difference method has been used.

We assume that plate of height $X_{\max}=100$, i.e. X varies from 0 to 100 and $Y_{\max}=25$ as corresponding to $Y \rightarrow \infty$, i.e. Y varies from 0 to 25. There are $m = 125$, and $n = 125$ equally spaced grid points in grid spacing in the X and Y direction, which means that $\Delta X, \Delta Y$ are constant mesh sizes along X and Y directions respectively and taken as follows;

$\Delta X = 0.8 (0 \leq X \leq 100), \Delta Y = 0.2 (0 \leq Y \leq 25)$ are constant mesh sizes. The time step is taken to be $\Delta \tau = 0.005$.

Let U', V', \bar{T}' denote the values of U, V, \bar{T} at the end of a time step respectively. Using the EFDA the following appropriate set of finite difference equations are obtained as;



Finite difference space grid.

$$\frac{U'_{i,j} - U'_{i-1,j}}{\Delta X} + \frac{V_{i,j} - V_{i,j-1}}{\Delta Y} = 0 \quad (13)$$

$$\frac{U'_{i,j} - U_{i,j}}{\Delta \tau} + U_{i,j} \frac{U_{i,j} - U_{i-1,j}}{\Delta X} + V_{i,j} \frac{U_{i,j+1} - U_{i,j}}{\Delta Y} = B \left(\frac{U_{i,j+1} - 2U_{i,j} + U_{i,j-1}}{(\Delta Y)^2} \right) \pm C \bar{T}_{i,j} - DU_{i,j} \quad (14)$$

$$\frac{\bar{T}'_{i,j} - \bar{T}_{i,j}}{\Delta \tau} + U_{i,j} \frac{\bar{T}_{i,j} - \bar{T}_{i-1,j}}{\Delta X} + V_{i,j} \frac{\bar{T}_{i,j+1} - \bar{T}_{i,j}}{\Delta Y} = F \left(\frac{\bar{T}_{i,j+1} - 2\bar{T}_{i,j} + \bar{T}_{i,j-1}}{(\Delta Y)^2} \right) \quad (15)$$

Where,

$$B = \frac{\rho_f}{\text{Re}(1-\phi)^{2.5} \{ (1-\phi)\rho_f + \phi\rho_s \}} \quad C = \frac{R_i(1-\phi)(\rho\beta)_f + \phi(\rho\beta)_s}{\beta_f(1-\phi)\rho_f + \phi\rho_s}$$

$$D = \frac{M\rho_f}{(1-\phi)\rho_f + \phi\rho_s} \quad F = \frac{k_{nf}/k_f}{\left[1 - \phi + \phi \frac{(\rho c_p)_s}{(\rho c_p)_f} \right] \text{Pr Re}}$$

With initial and boundary conditions:

$$U_{i,j}^0 = 0, V_{i,j}^0 = 0, \bar{T}_{i,j}^0 = 0 \quad (16)$$

$$U_{0,j}^n = 0, V_{0,j}^n = 0, \bar{T}_{0,j}^n = 0$$

$$U_{i,0}^n = 0, V_{i,0}^n = 0, \bar{T}_{i,0}^n = 1 \quad (17)$$

$$U_{i,L}^n = 1, V_{i,L}^n = 0, \bar{T}_{i,L}^n = 0 \quad \text{where } L \rightarrow \infty$$

3.1. Stability and Convergence Analysis

Since an explicit method is used in time, the analyses of stability and convergence of the finite difference scheme are discussed.

Let,

$$U = \Psi(\tau)e^{i\alpha x}e^{i\beta y}$$

$$\bar{T} = \theta(\tau)e^{i\alpha x}e^{i\beta y} \quad (18)$$

After the time step these terms will becomes;

$$U' = \Psi'(\tau)e^{i\alpha x}e^{i\beta y}$$

$$\bar{T}' = \theta'(\tau)e^{i\alpha x}e^{i\beta y} \quad (19)$$

Then (14) becomes;

$$\frac{\Psi'(\tau)e^{i\alpha x}e^{i\beta y} - \Psi(\tau)e^{i\alpha x}e^{i\beta y}}{\Delta \tau} + U \frac{\Psi(\tau)e^{i\alpha x}e^{i\beta y} - \Psi(\tau)e^{i\alpha(x-\Delta x)}e^{i\beta y}}{\Delta X} + V \frac{\Psi(\tau)e^{i\alpha x}e^{i\beta(y+\Delta y)} - \Psi(\tau)e^{i\alpha x}e^{i\beta y}}{\Delta Y} = B \left(\frac{\Psi(\tau)e^{i\beta\Delta y} - 2\Psi(\tau) + \Psi(\tau)e^{-i\beta\Delta y}}{(\Delta Y)^2} \right) \pm e^{-i\alpha x}e^{-i\beta y}(C\bar{T} - DU)$$

$$= B \frac{\Psi(\tau)e^{i\alpha x}e^{i\beta(y+\Delta y)} - 2\Psi(\tau)e^{i\alpha x}e^{i\beta y} + \Psi(\tau)e^{i\alpha x}e^{i\beta(y-\Delta y)}}{(\Delta Y)^2} \pm C\bar{T} - DU$$

$$\Rightarrow \frac{\Psi'(\tau) - \Psi(\tau)}{\Delta \tau} + U \frac{\Psi(\tau) - \Psi(\tau)e^{-i\alpha\Delta x}}{\Delta X} + V \frac{\Psi(\tau)e^{i\beta\Delta y} - \Psi(\tau)}{\Delta Y} = B \frac{\Psi(\tau)e^{i\beta\Delta y} - 2\Psi(\tau) + \Psi(\tau)e^{-i\beta\Delta y}}{(\Delta Y)^2} \pm e^{-i\alpha x}e^{-i\beta y}(C\bar{T} - DU)$$

$$\Rightarrow \frac{\Psi'(\tau) - \Psi(\tau)}{\Delta \tau} + U \frac{\Psi(\tau)(1 - e^{-i\alpha\Delta x})}{\Delta X} + V \frac{\Psi(\tau)(e^{i\beta\Delta y} - 1)}{\Delta Y} = B \frac{\Psi(\tau)(e^{i\beta\Delta y} + e^{-i\beta\Delta y} - 2)}{(\Delta Y)^2} \pm e^{-i\alpha x}e^{-i\beta y}(C\bar{T} - DU)$$

$$\Rightarrow \frac{\Psi'(\tau) - \Psi(\tau)}{\Delta \tau} + U \frac{\Psi(\tau)(1 - e^{-i\alpha\Delta x})}{\Delta X} + V \frac{\Psi(\tau)(e^{i\beta\Delta y} - 1)}{\Delta Y} = B \frac{\Psi(\tau)(e^{i\beta\Delta y} + e^{-i\beta\Delta y} - 2)}{(\Delta Y)^2} \pm e^{-i\alpha x}e^{-i\beta y}(C\bar{T} - DU)$$

$$\Rightarrow \frac{\Psi'(\tau) - \Psi(\tau)}{\Delta \tau} + U \frac{\Psi(\tau)(1 - e^{-i\alpha\Delta x})}{\Delta X} + V \frac{\Psi(\tau)(e^{i\beta\Delta y} - 1)}{\Delta Y} = B \frac{\Psi(\tau)(e^{i\beta\Delta y} + e^{-i\beta\Delta y} - 2)}{(\Delta Y)^2} \pm e^{-i\alpha x}e^{-i\beta y}(C\bar{T} - DU)$$

$$\Rightarrow \frac{\Psi'(\tau) - \Psi(\tau)}{\Delta \tau} + U \frac{\Psi(\tau)(1 - e^{-i\alpha\Delta x})}{\Delta X} + V \frac{\Psi(\tau)(e^{i\beta\Delta y} - 1)}{\Delta Y} = B \frac{\Psi(\tau)(2\text{Cos}\beta\Delta y - 2)}{(\Delta Y)^2} \pm e^{-i\alpha x}e^{-i\beta y}(C\bar{T} - DU)$$

$$\Rightarrow \frac{\Psi'(\tau) - \Psi(\tau)}{\Delta \tau} + U \frac{\Psi(\tau)(1 - e^{-i\alpha\Delta x})}{\Delta X} + V \frac{\Psi(\tau)(e^{i\beta\Delta y} - 1)}{\Delta Y} = B \frac{2\Psi(\tau)(\text{Cos}\beta\Delta y - 1)}{(\Delta Y)^2} \pm \frac{\Psi(\tau)}{U}(C\bar{T} - DU) \quad (20)$$

and (15) becomes;

$$\frac{\theta'(\tau)e^{i\alpha x}e^{i\beta y} - \theta(\tau)e^{i\alpha x}e^{i\beta y}}{\Delta \tau} + U \frac{\theta(\tau)e^{i\alpha x}e^{i\beta y} - \theta(\tau)e^{i\alpha(x-\Delta x)}e^{i\beta y}}{\Delta X} + V \frac{\theta(\tau)e^{i\alpha x}e^{i\beta(y+\Delta y)} - \theta(\tau)e^{i\alpha x}e^{i\beta y}}{\Delta Y} = F \frac{\theta(\tau)e^{i\alpha x}e^{i\beta(y+\Delta y)} - 2\theta(\tau)e^{i\alpha x}e^{i\beta y} + \theta(\tau)e^{i\alpha x}e^{i\beta(y-\Delta y)}}{(\Delta Y)^2}$$

$$\Rightarrow \frac{\theta'(\tau) - \theta(\tau)}{\Delta \tau} + U \frac{\theta(\tau) - \theta(\tau)e^{-i\alpha\Delta x}}{\Delta X} + V \frac{\theta(\tau)e^{i\beta\Delta y} - \theta(\tau)}{\Delta Y} = F \frac{\theta(\tau)e^{i\beta\Delta y} - 2\theta(\tau) + \theta(\tau)e^{-i\beta\Delta y}}{(\Delta Y)^2}$$

$$\Rightarrow \frac{\theta'(\tau) - \theta(\tau)}{\Delta\tau} + U \frac{\theta(\tau)(1 - e^{i\alpha\Delta x})}{\Delta X} +$$

$$V \frac{\theta(\tau)(e^{i\beta\Delta y} - 1)}{\Delta Y} = F \frac{\theta(\tau)(e^{i\beta\Delta y} + e^{-i\beta\Delta y} - 2)}{(\Delta Y)^2}$$

$$\Rightarrow \frac{\theta'(\tau) - \theta(\tau)}{\Delta\tau} + U \frac{\theta(\tau)(1 - e^{-i\alpha\Delta x})}{\Delta X} +$$

$$V \frac{\theta(\tau)(e^{i\beta\Delta y} - 1)}{\Delta Y} = F \frac{\theta(\tau)(2 \frac{e^{i\beta\Delta y} + e^{-i\beta\Delta y}}{2} - 2)}{(\Delta Y)^2}$$

$$\Rightarrow \frac{\theta'(\tau) - \theta(\tau)}{\Delta\tau} + U \frac{\theta(\tau)(1 - e^{-i\alpha\Delta x})}{\Delta X} +$$

$$V \frac{\theta(\tau)(e^{i\beta\Delta y} - 1)}{\Delta Y} = F \frac{\theta(\tau)(2 \cdot \text{Cas}\beta\Delta y - 2)}{(\Delta Y)^2}$$

$$\Rightarrow \frac{\theta'(\tau) - \theta(\tau)}{\Delta\tau} + U \frac{\theta(\tau)(1 - e^{-i\alpha\Delta x})}{\Delta X} +$$

$$V \frac{\theta(\tau)(e^{i\beta\Delta y} - 1)}{\Delta Y} = F \frac{2\theta(\tau)(\text{Cas}\beta\Delta y - 1)}{(\Delta Y)^2} \quad (21)$$

Then (20) and (21) can be write as;

$$\Psi' = P\Psi \quad (22)$$

$$\theta' = Q\theta \quad (23)$$

Where,

$$P = 1 + \Delta\tau \left[B \frac{2}{\Delta Y^2} (\cos \beta\Delta y - 1) - \right.$$

$$\left. U \frac{(1 - e^{-i\alpha\Delta x})}{\Delta X} - V \frac{(e^{i\beta\Delta y} - 1)}{\Delta Y} + \frac{1}{U} (C\bar{T} - DU) \right]$$

$$Q = 1 + \Delta\tau \left[F \frac{2}{\Delta Y^2} (\cos \beta\Delta y - 1) - \right.$$

$$\left. U \frac{(1 - e^{-i\alpha\Delta x})}{\Delta X} - V \frac{(e^{i\beta\Delta y} - 1)}{\Delta Y} \right]$$

Hence equations (22) and (23) can be expressed in matrix notation as, and these equations are;

$$\begin{bmatrix} \Psi' \\ \theta' \end{bmatrix} = \begin{bmatrix} P & 0 \\ 0 & Q \end{bmatrix} \begin{bmatrix} \Psi \\ \theta \end{bmatrix}$$

That is, $\eta' = T\eta$

where,

$$\eta' = \begin{bmatrix} \Psi' \\ \theta' \end{bmatrix}, T = \begin{bmatrix} P & 0 \\ 0 & Q \end{bmatrix} \text{ and } \eta = \begin{bmatrix} \Psi \\ \theta \end{bmatrix}$$

After simplification of the matrix T, we get the following eigenvalues, $\lambda_1 = P, \lambda_2 = Q$; P, Q are matrices but λ_1, λ_2 scalar numbers.

For stability, each eigenvalues λ_1, λ_2 must not exceed unity in modulus. Hence the stability condition is;

$$|P| \leq 1, |Q| \leq 1$$

Now we assume that U is everywhere non-negative and V is everywhere non-positive. Thus;

$$Q = 1 + \Delta\tau \left[F \frac{2}{\Delta Y^2} - U \frac{2}{\Delta X} - V \frac{2}{\Delta Y} \right]$$

$$\Rightarrow Q = 1 + 2(2Fc - a - b)$$

$$\text{Where, } a = U \frac{\Delta\tau}{\Delta X}, b = V \frac{\Delta\tau}{\Delta Y}, c = \frac{\Delta\tau}{\Delta Y^2}$$

The coefficients a, b and c are all real and nonnegative. We can demonstrated that the maximum modulus of Q occurs when $\alpha\Delta X = m\pi$ and $\beta\Delta Y = n\pi$, where m and n are integers and hence Q is real. The value of $|Q|$ is greater when both m and n are odd integers.

To satisfy the second condition $|Q| \leq 1$, the most negative allowable values is $Q = -1$. Therefore the first stability condition is;

$$|1 + 2(2Fc - a - b)| \leq 1,$$

$$\Rightarrow -1 \leq 1 + 2(2Fc - a - b)$$

$$\Rightarrow -2 \leq 2(2Fc - a - b)$$

$$\Rightarrow -1 \leq (2Fc - a - b)$$

Since from the initial condition, $U = V = \bar{T} = 0$ at $\tau = 0$,

We get,

$$1 \geq 2Fc$$

$$\Rightarrow 1 \geq 2 \frac{\Delta\tau}{\Delta Y^2} \cdot \frac{k_{nf}/k_f}{\left[1 - \phi + \phi \frac{(\rho c_p)_s}{(\rho c_p)_f} \right] \text{Pr Re}}$$

At $\tau = 0$ consideration due to stability and convergence analysis is if $\phi \leq 0.7$
 $\text{Re} \geq 0.3937, \text{Pr} \geq 3.84$.

4. RESULTS AND DISCUSSION

In this section, numerical results of flow profiles for various values of Prandtl number (Pr), Magnetic

Table 1: Thermo Physical Properties of Base Fluids and Nanoparticles [11]

Physical Properties	Water (Base Fluid)	Ethylene Glycol (Base Fluid)	Cu	Ag	Al ₂ O ₃	TiO ₃
C_p (J/Kg-K)	4179	2428	385	235	765	686.2
ρ (Kg/m ³)	997.1	1115	8933	10500	3970	4250
k (W/m-K)	0.613	0.253	401	429	40	8.9538
$\beta \times 10^{-5}$ (K ⁻¹)	21	0.65	1.67	1.89	0.85	0.9

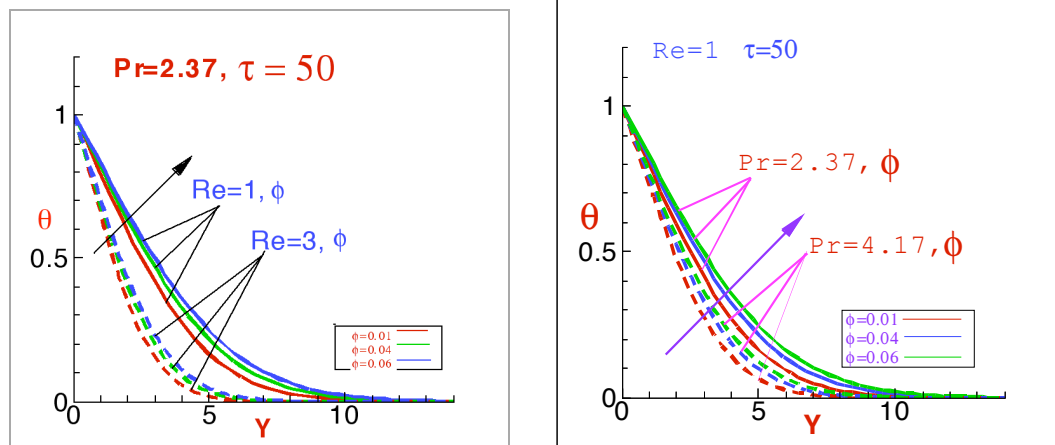


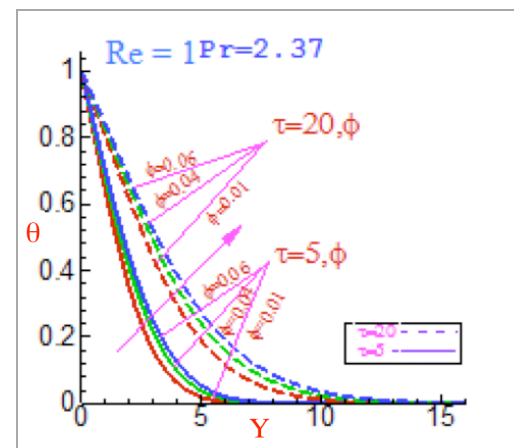
Figure 2: Effect of Re and Pr on temperature profile.

parameter (M), Richardson number (Ri), Reynolds number (Re), volume fraction of nanofluids (ϕ) are displayed.

Here we see that the velocity profile and temperature profile does not show any change after non-dimensional time, $\tau=150$. So we say that the solution for $\tau > 150$ is steady state solution.

Figures (2-3), here the graphical representations of the temperature for three different variable quantities Prandtl number (Pr), non-dimensional time (τ) and Reynolds number (Re). It is found that the thermal boundary layer thickness is decreasing when Prandtl number (Pr) increasing so we can say that thermal diffusivity is small, since the thickness of boundary layer for velocity is increasing, kinematic viscosity is large. When the volume fraction of copper nanoparticles is increased, the velocity of the fluid is also increasing. The reason is high thermal conductivity of copper nanoparticles, which enhances conductive heat transfer mechanism.

For the high Reynolds number, the thickness of the boundary layer for both thermal and velocity have been increased so low viscosity had been arose.

Figure 3: Effect of τ with various values of ϕ on temperature profile.

Figures (4-5), the velocity distribution are plotted respectively for different values of volume fraction of nanofluids (ϕ) and Magnetic parameter (M) with the values of $Re=0.5$, $Ri=2$ and $Pr=3.39$. These graphs declare that, when Magnetic parameter is increased with different values of volume fraction ($\phi=0.1, 0.2, 0.5$) the velocity boundary layer thickness is decreasing but after the point of separation boundary layer thickness is increasing. The momentum boundary layer thickness decreases with the increases in ϕ for both the

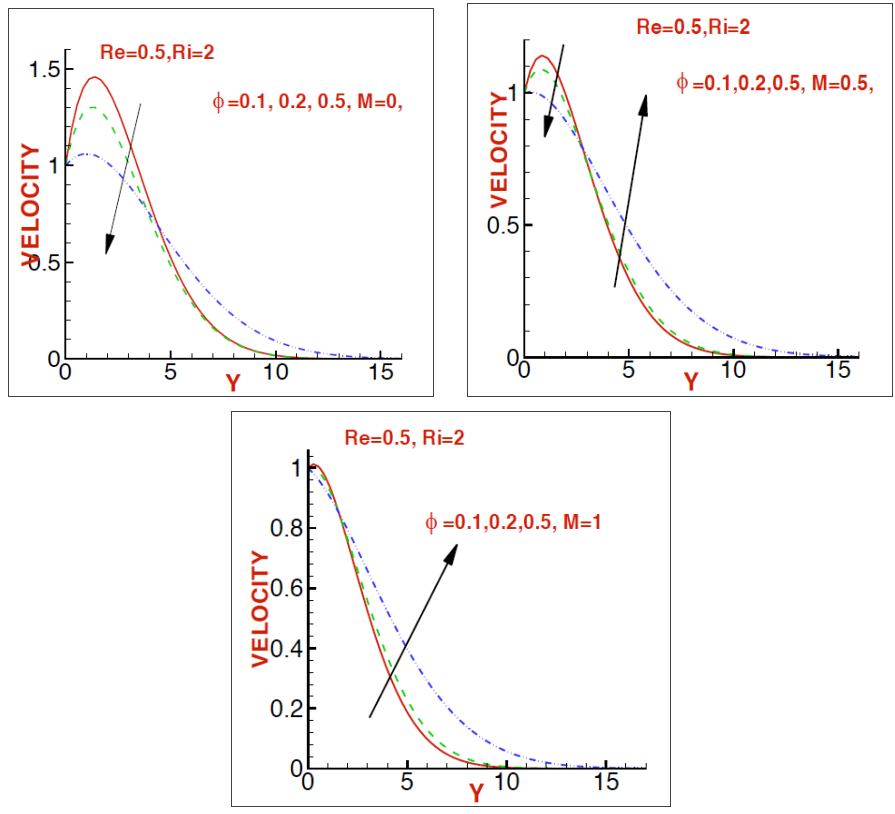


Figure 4: Effect of ϕ with various values of M on velocity profile.

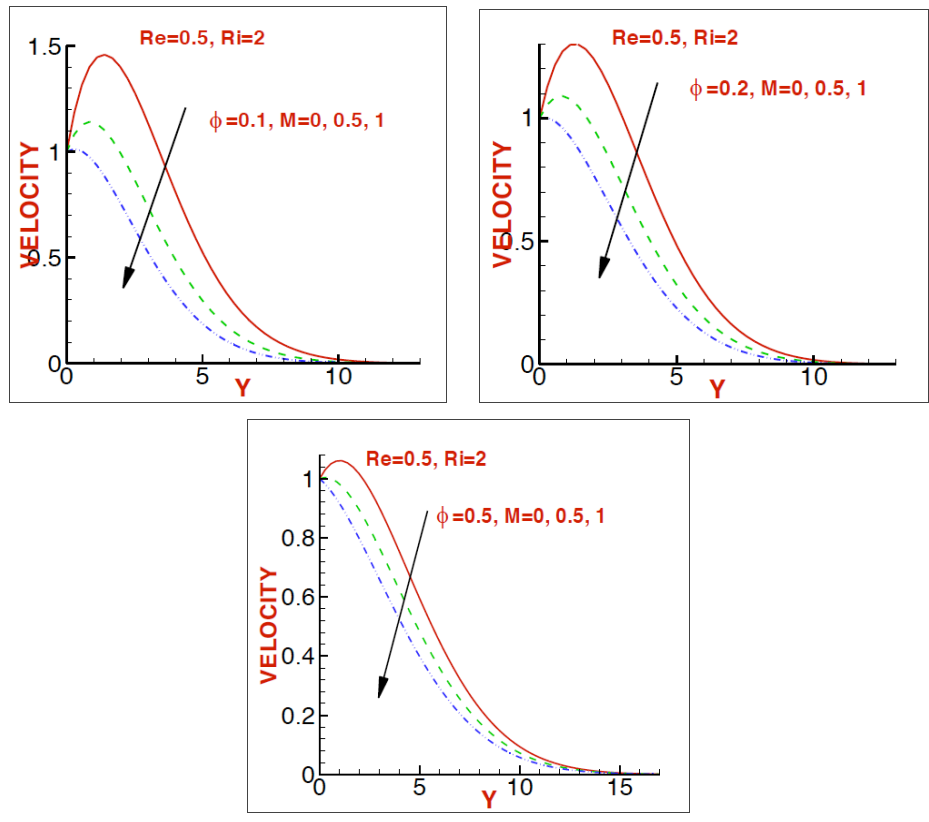


Figure 5: Effect of M with various of ϕ on velocity profile.

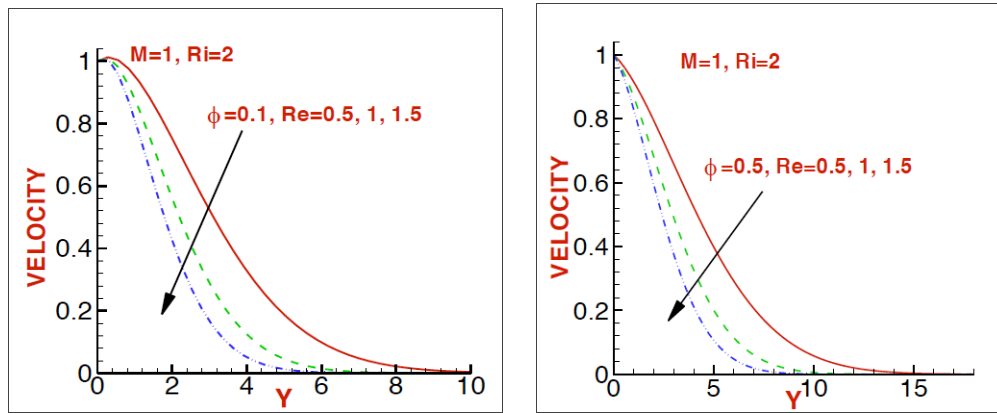


Figure 6: Effect of Re with various of ϕ on velocity profile.

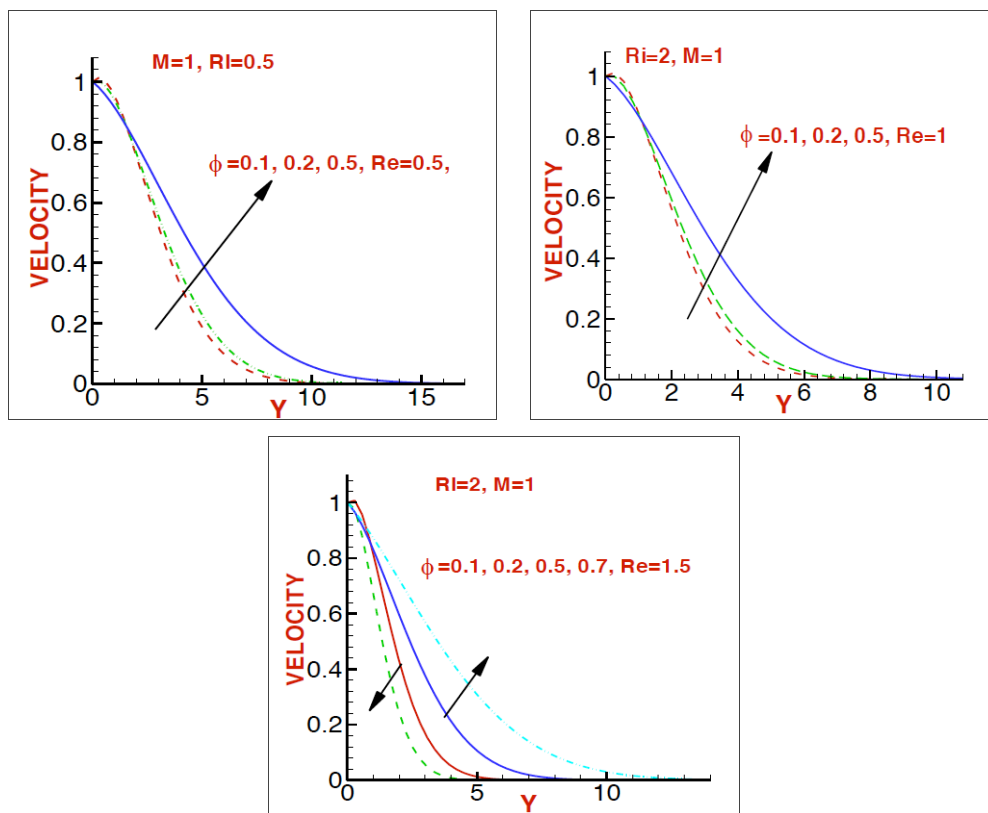


Figure 7: Effect of Re with various of ϕ on velocity profile.

presence ($M=0.5,1$) and the absence ($M=0$) of the magnetic field. It is also seen that the magnetic field effects leads to more thinning of the boundary layer. The phenomenon is due to fact that the variation of M leads to the variation of Lorentz force, due to the magnetic field and the Lorentz force produces resistance to the transport phenomena.

Figures (6-7), the velocity distribution are plotted respectively for different values of volume fraction of nanofluids (ϕ) and Reynolds number (Re) with the

values of $M=1, Ri=2$ and $Pr=3.39$. These graphs has been shown that, when Reynolds number is increased with different values of volume fraction ($\phi=0.1, 0.2, 0.5$) the velocity boundary layer thickness is decreasing. Since Re is small viscous force is high and if Re is large we have stagnation point.

Figures (8-9), depict the effect of volume fraction of nanofluids (ϕ) and Richardson number (Ri) with the values of $M=1, Re=0.5$ and $Pr=3.39$. It is seen that,

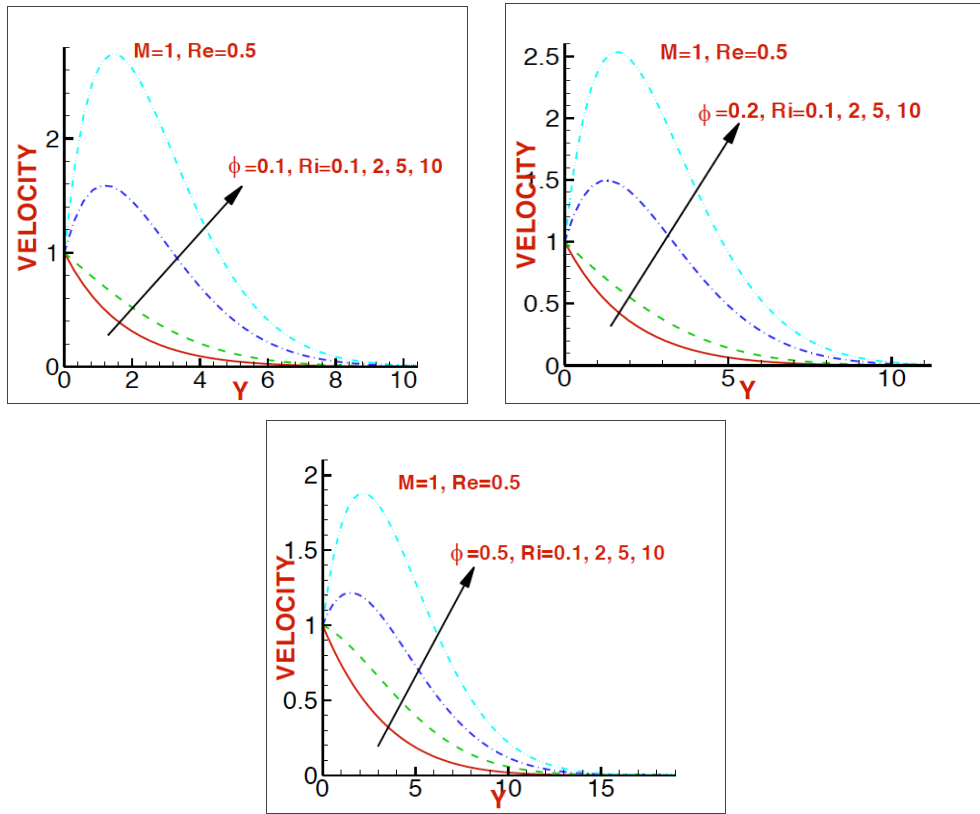


Figure 8: Effect of ϕ with various of Ri on velocity profile.

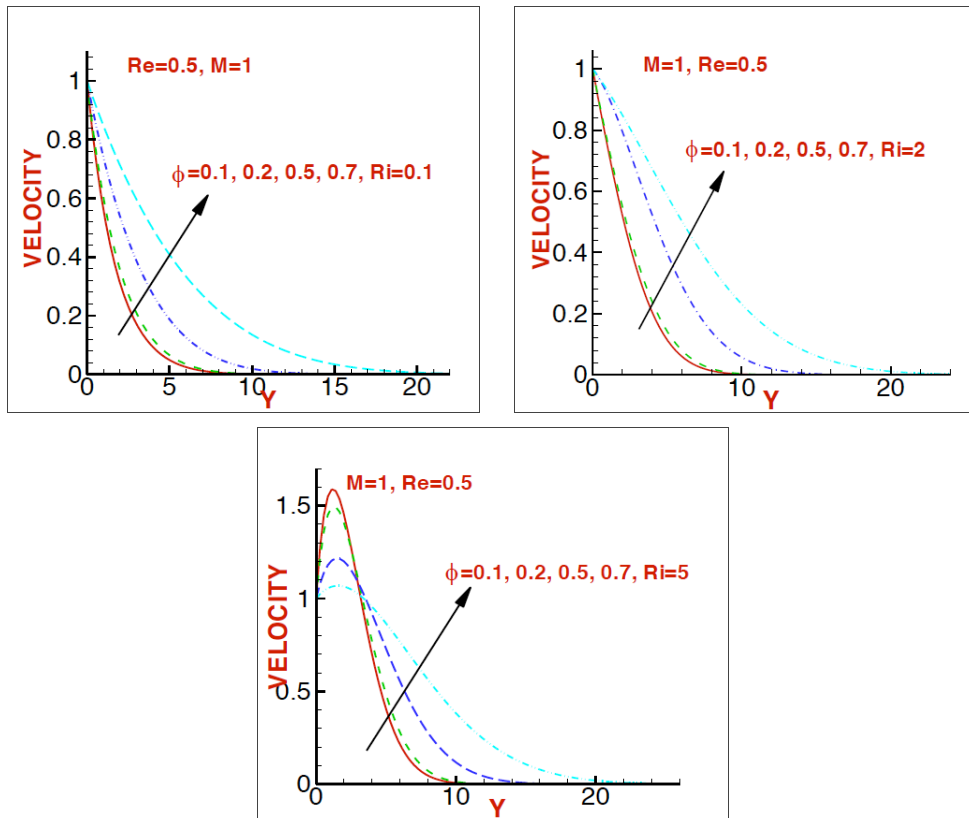


Figure 9: Effect of ϕ with various of Ri on velocity profile.

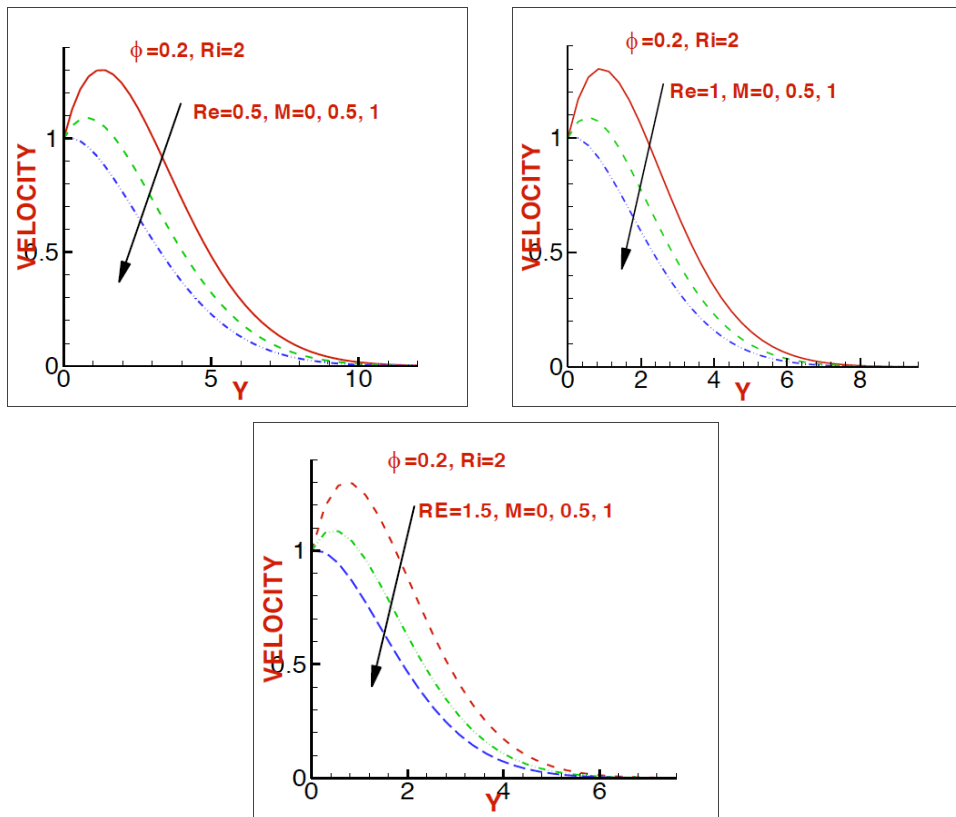


Figure 10: Effect of M with various of Re on velocity profile.

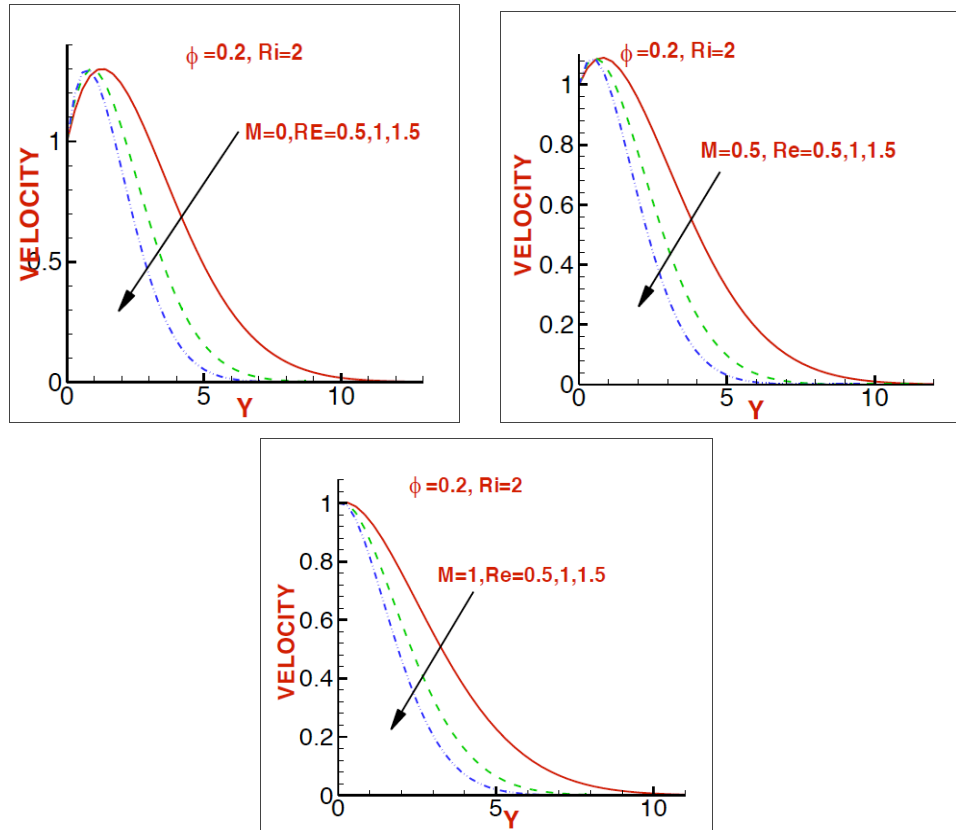


Figure 11: Effect of Re with various of M on velocity profile.

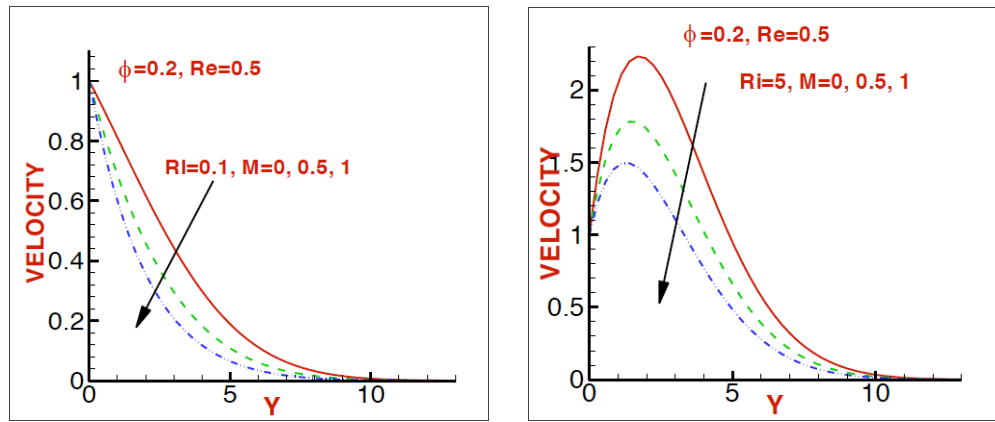


Figure 12: Effect of M with various of Ri on velocity profile.

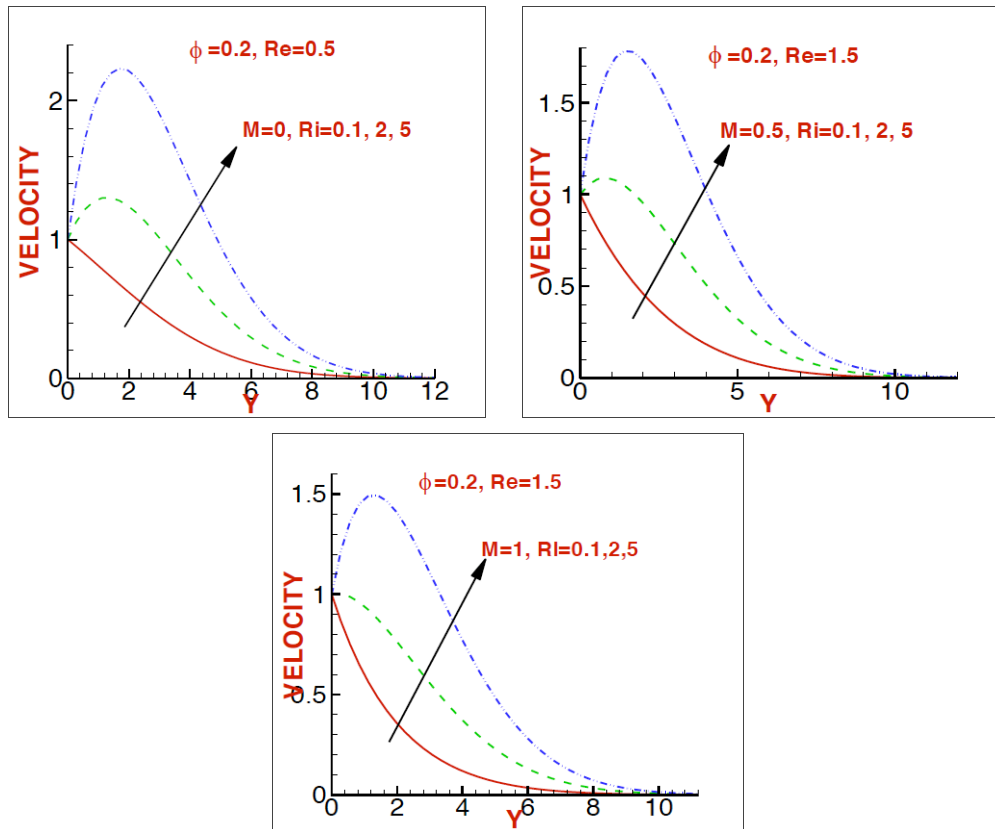


Figure 13: Effect of Ri with various of M on velocity profile.

when Richardson number is increased with different values of volume fraction ($\phi=0.1, 0.2, 0.5$) the velocity boundary layer thickness is increasing and volume fraction is increased with different values of Richardson number ($Ri=0.1, 2, 5$) the velocity boundary layer thickness is also increasing. That means there is a low shear stress on the wall and more natural convection, which follows the reduction in the velocity gradient. As Ri increases, buoyancy motions dominate the forced motions near the bottom wall.

Figures (10-13), show the effect of Reynolds number (Re) and Richardson number (Ri) with the values of $M=1$, $\phi=0.2$ and $Pr=3.39$. It is seen that, when Richardson number is increased with different values of Magnetic parameter ($M=0, 0.5, 1$) the velocity boundary layer thickness is increasing and Reynolds number is increased with different values of Magnetic parameter ($M=0, 0.5, 1$), the velocity boundary layer thickness is thinning.

Figures (14-17), show the effects of Magnetic parameter (M), Richardson number (Ri), Reynolds number (Re) and volume fraction of nanofluids (ϕ). It is seen that, when Magnetic parameter (M), Richardson number (Ri), Reynolds number (Re), volume fraction of nanofluids (ϕ) are increasing with different values the velocity boundary layer thickness are increasing for ϕ , Ri and velocity boundary layer thickness are decreasing for Re, M.

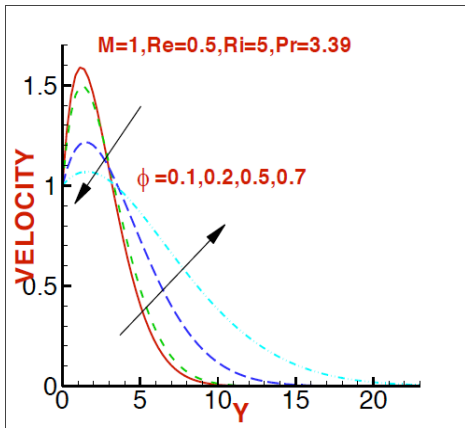


Figure 14: Effect of ϕ with on velocity profile.

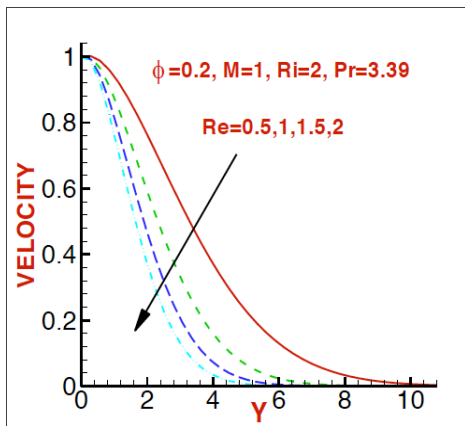


Figure 15: Effect of ϕ Re velocity profile.

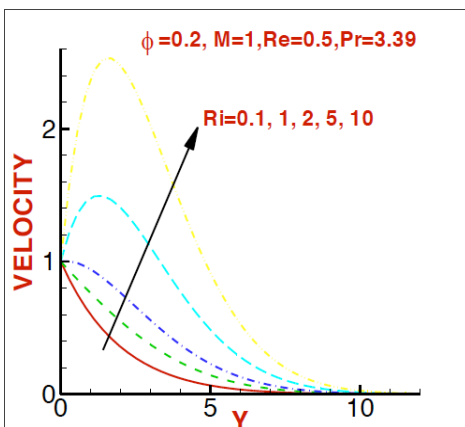


Figure 16: Effect of Ri on velocity profile.

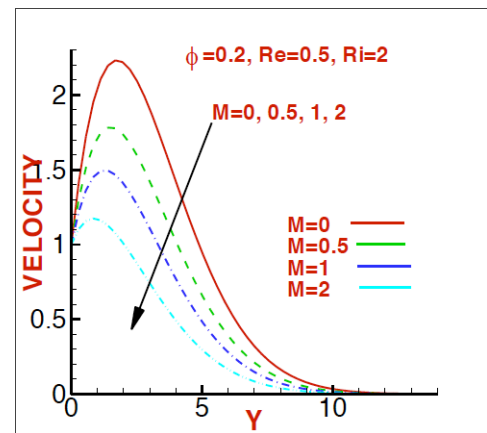


Figure 17: Effect of M on velocity profile.

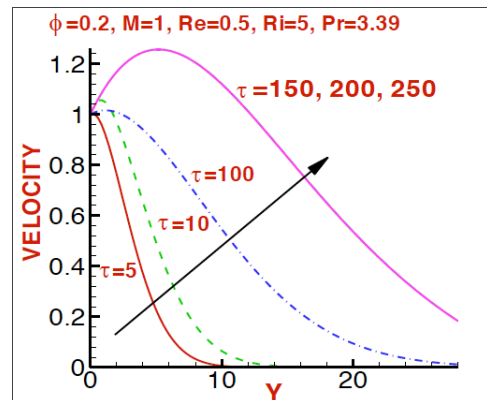
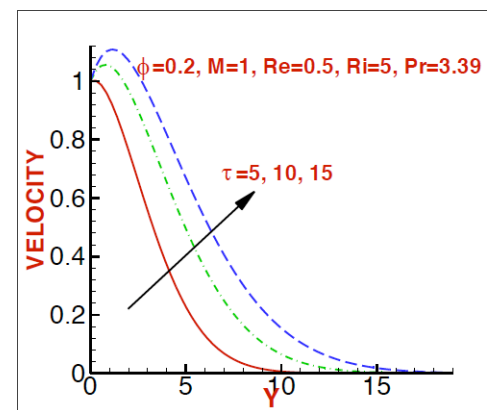


Figure 18: Effect of τ on velocity profile.

Figures (18-19), show the effect of non- dimensional time (τ) with the values of $M=1$, $\phi=0.2$, $Re=0.5$, $Ri=2$ and $Pr=3.39$, use water and Ethylene Glycol as base fluids. It is seen that, non- dimensional time (τ) is increased the velocity boundary layer thickness is increasing. But when $\tau > 150$ the profiles does not show any change that is after $\tau=150$ we get steady state motion. Also we compare the effect of τ with Cu-Water and Cu-EG. It is obvious that, boundary layer thickness changes with the change of base fluid and the effects of Cu-EG is greater than Cu-Water.

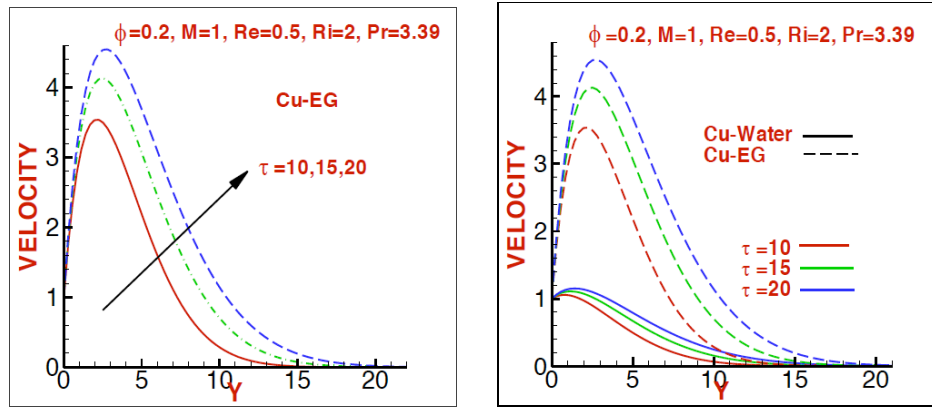


Figure 19: Effect of τ on velocity profile with different base fluids.

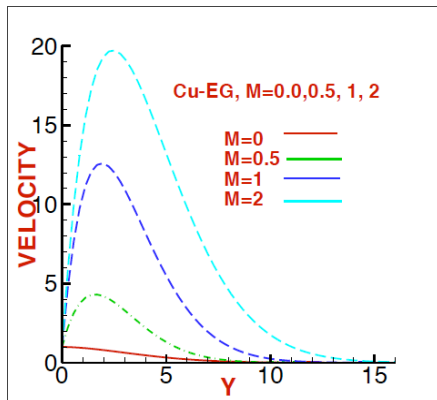


Figure 20: Effect of Cu-EG on velocity profile.

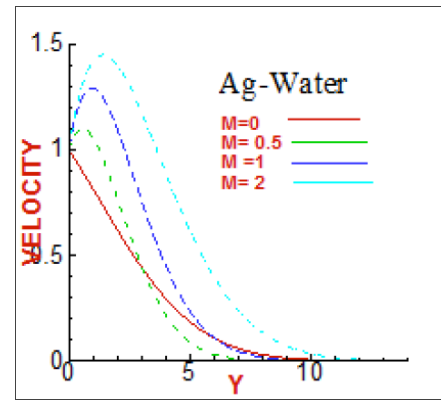


Figure 23: Effect of Ag-Water on velocity profile.

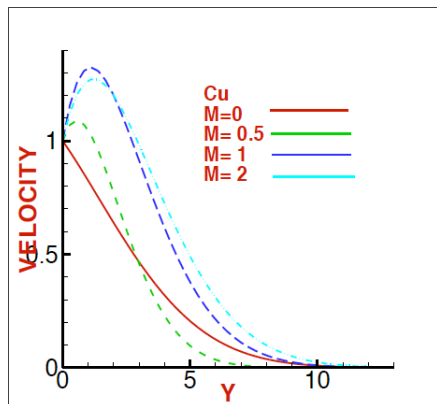


Figure 21: Effect of Cu-Water on velocity profile.

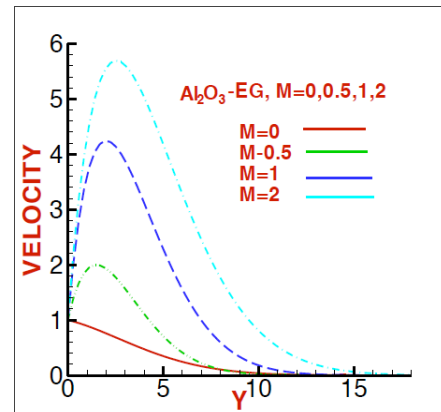


Figure 24: Effect of Al_2O_3 -EG on velocity profile.

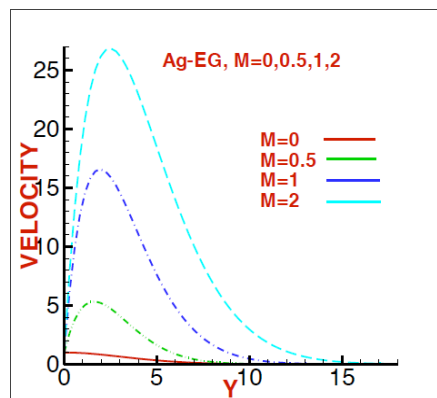


Figure 22: Effect of Ag-EG on velocity profile.

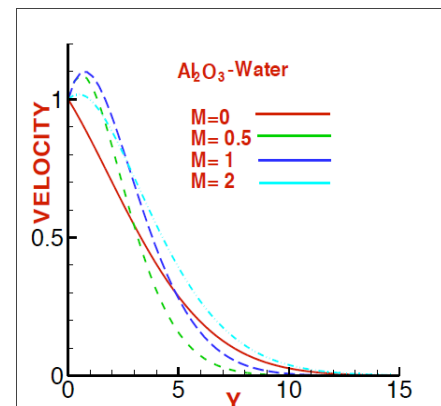


Figure 25: Effect of Al_2O_3 -water on velocity profile.

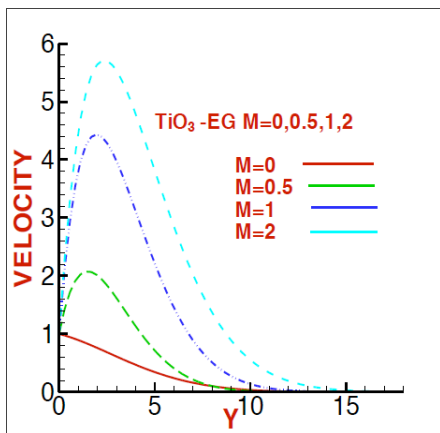


Figure 26: Effect of TiO₃-EG on velocity profile.

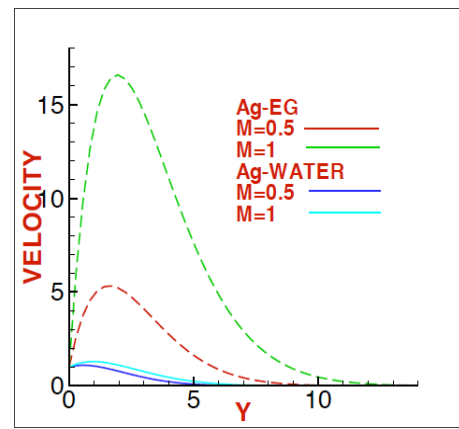


Figure 29: Effect of Ag in water and EG.

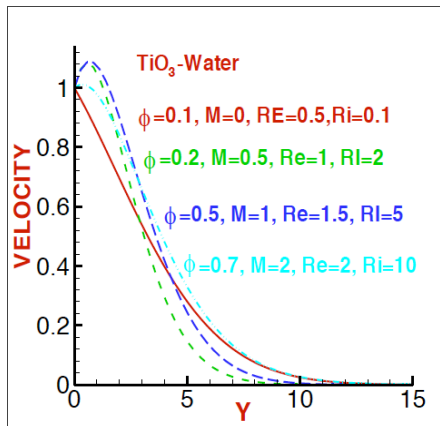


Figure 27: Effect of TiO₃-water on velocity profile.

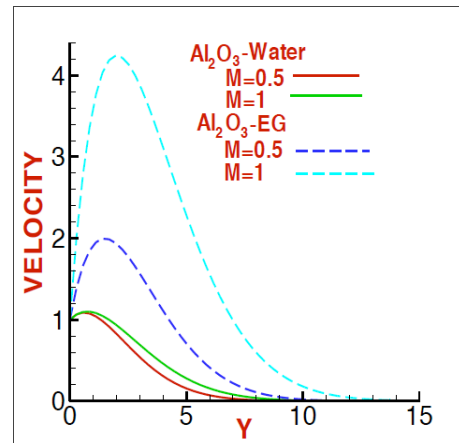


Figure 30: Effect of Al₂O₃ in water and EG.

Figures (20-27), we compare the effect of various four types of used nanoparticles such as Cu, Ag, Al₂O₃, TiO₃ with pure water and Ethylene Glycol. We use (M=0, $\phi=0.1$, Re=0, Ri=0.1; M=0.5, $\phi=0.2$, Re=1, Ri=2; M=1, $\phi=0.5$, Re=1.5, Ri=5; M=2, $\phi=0.7$, Re=2, Ri=10) It has been seen that, boundary layer thickness changes with the change of nanoparticles types. The main reason of this variation is different physical and mechanical properties of nanoparticles such as dynamic viscosity, density and expansion coefficients.

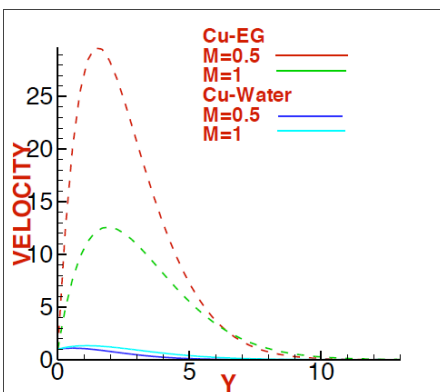


Figure 28: Effect of Cu in water and EG.

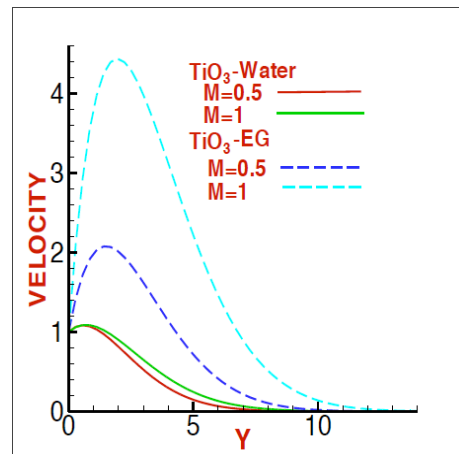


Figure 31: Effect of TiO₃ in water and EG.

Figures (28-31) is presented to show the effects of nanoparticles in different base fluids such as pure water and Ethylene Glycol in same profile. We use M=0.5, $\phi=0.2$, Re=1, Ri=2; M=1, $\phi=0.5$, Re=1.5, Ri=5; the boundary layer is increasing much higher in the base fluid of Ethylene Glycol than that of base fluid of water.

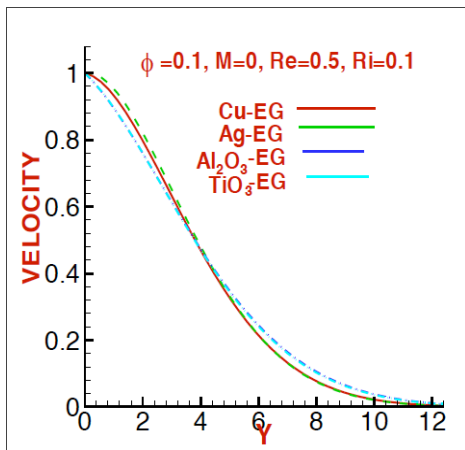


Figure 32: Effect of nanoparticles in EG.

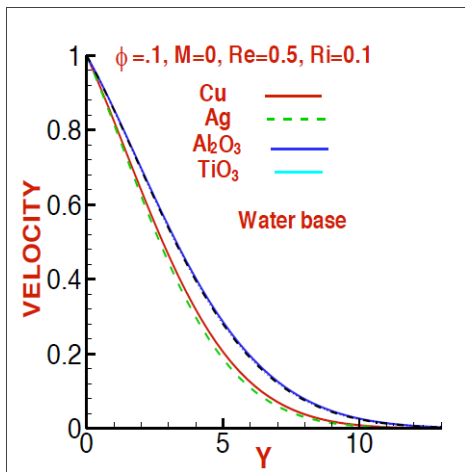


Figure 33: Effect of nanoparticles in water.

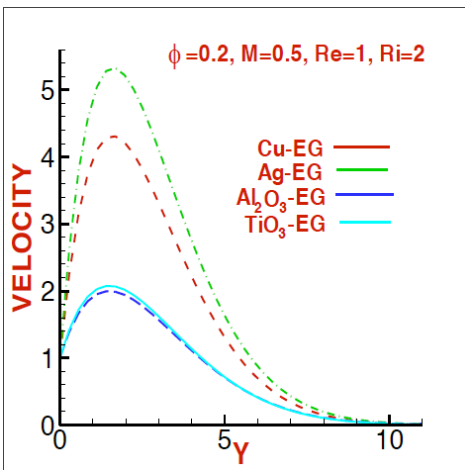


Figure 34: Effect of nanoparticles in EG.

Figures (32-39) show the variations of different nanoparticles in same profile with various values of ϕ , M , Re , Ri and using two base fluids (pure water and Ethylene glycol).

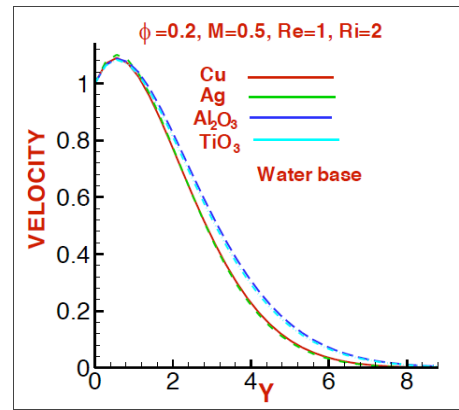


Figure 35: Effect of nanoparticles in water.

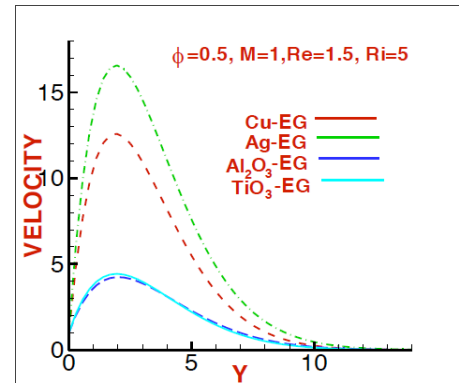


Figure 36: Effect of nanoparticles in EG.

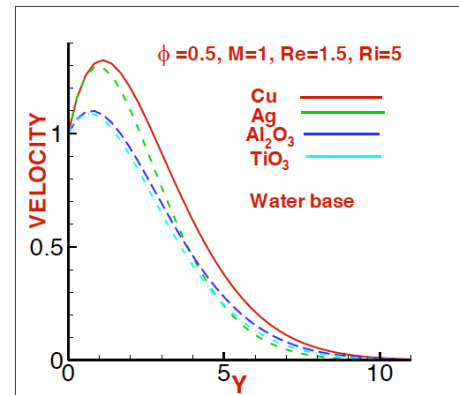


Figure 37: Effect of nanoparticles in water.

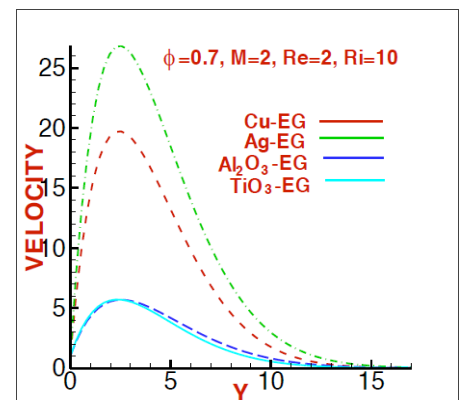


Figure 38: Effect of nanoparticles in EG.

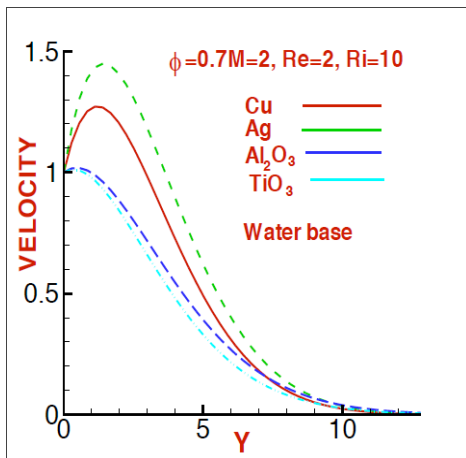


Figure 39: Effect of nanoparticles in water.

Figures (40-41) show the steady state and unsteady state of nanoparticles (Cu) with various values of ϕ , M , Re , Ri and using two base fluids (pure water and Ethylene glycol) and seen that velocity has larger motion in the case of unsteady than that of steady case. But opposite on Cu-EG.

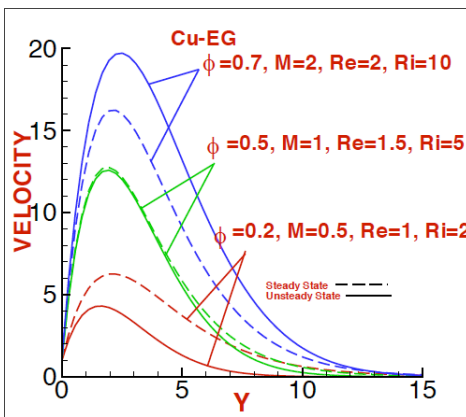


Figure 40: Steady and unsteady state of Cu-water.

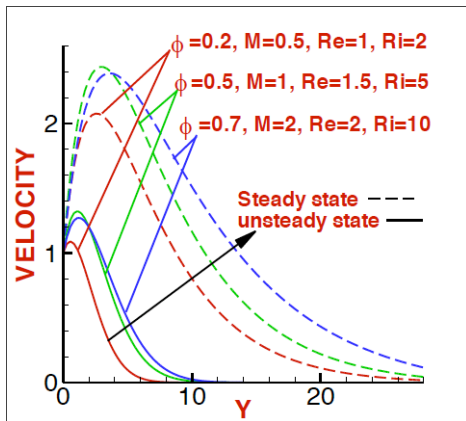


Figure 41: Steady and unsteady state of Cu-EG.

Figures (42-43) shows the steady state and unsteady state of nanoparticles (Cu) with various values of ϕ , M , Re , Ri and using two base fluids (pure water and Ethylene glycol) on velocity and temperature profiles. It is observed that steady state solution induced more flow than that of unsteady state.

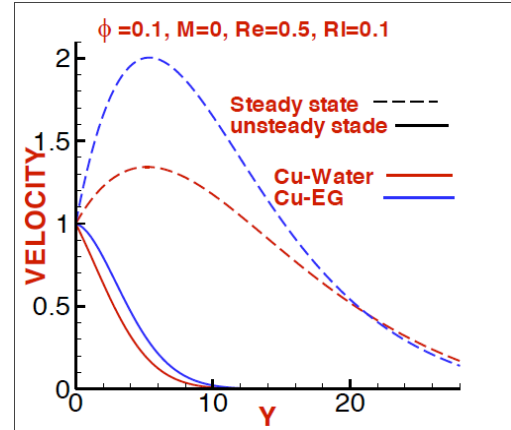


Figure 42: Steady and unsteady state of Cu.

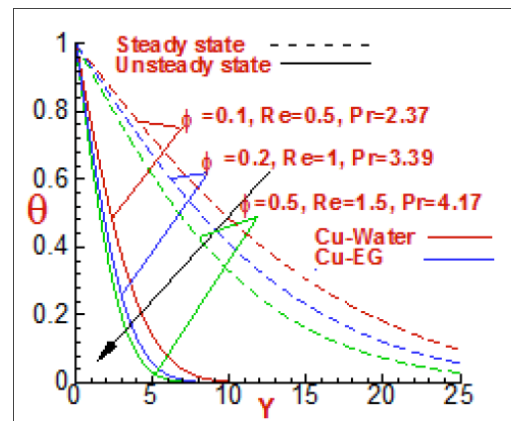


Figure 43: Steady and unsteady state of Cu-water.

Figures (44) indicates the effect of shearing stress with respect to volume fraction (ϕ) for different values of Re , M , Pr , Ri at the wall that means $Y=0$ and we have taken $\phi=0.0, 0.1, 0.2, 0.5, 0.7$. Increasing the values of Re , M , Pr shearing stress is decreasing and shearing stress is increasing if Ri is increasing.

Figures (45) indicates the effect of Nusselt number with respect to volume fraction (ϕ) for different values of Re , M , Pr , Ri at the wall that means $Y=0$ and we have taken $\phi=0.0, 0.1, 0.2, 0.5, 0.7$. Increasing the values of M shearing stress is decreasing and shearing stress is increasing if Re , Pr , Ri is increasing.

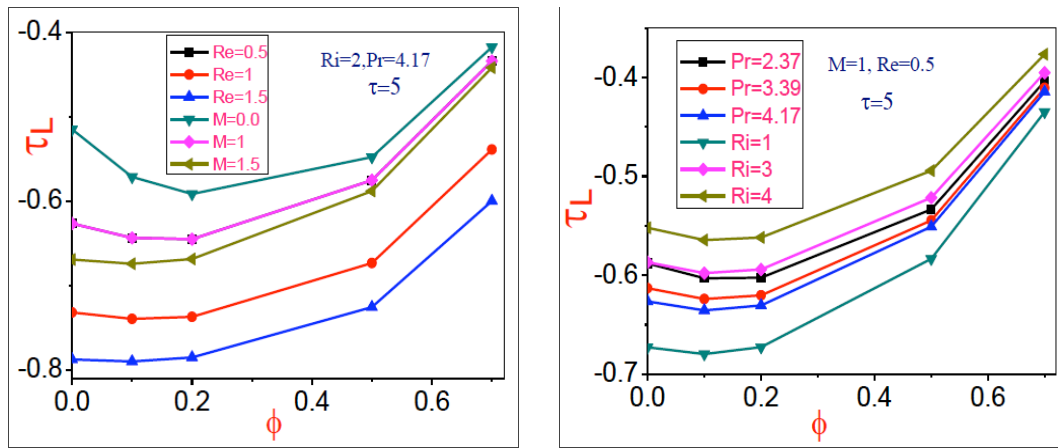


Figure 44: Profiles of shearing stress with different values of parameter around the wall.

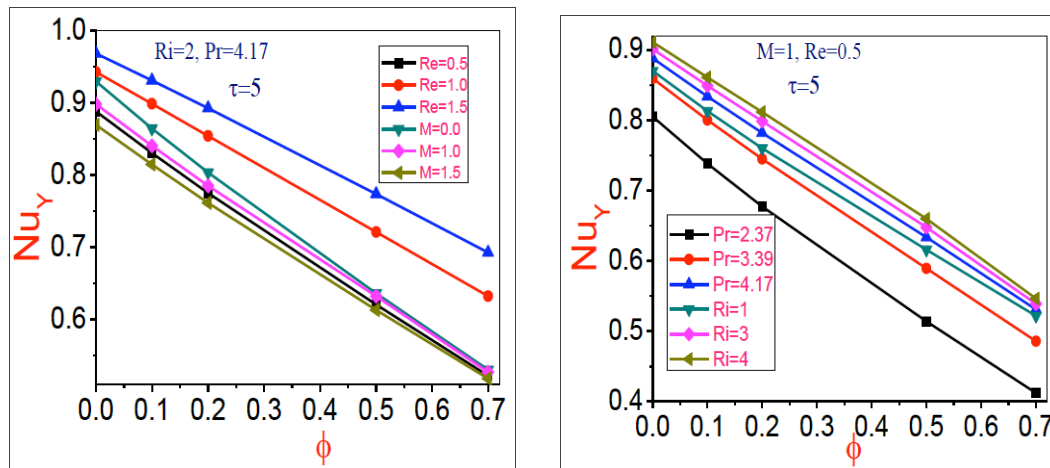


Figure 45: Profiles of Nusselt number with different values of parameter around the wall.

CONCLUSION

The problem of convective heat transfer in a magnetic field with water and Ethylene Glycol base fluid, nanofluid particles has been studied numerically. Various aspect ratios and Prandtl numbers have been considered for the velocity and temperature fields. The explicit finite difference technique with stability and convergence analysis has been employed as a solution tools to complete the formulation of the model. The results of the numerical analysis lead to the following conclusions:

1. The presence of magnetic field makes the momentum boundary layer thickener.
2. The thickness of boundary layer for the steady state is higher than that of the unsteady state.
3. The velocity and temperature profiles depend on parameters.

4. The shape of boundary layer is changed with the change of base fluids; and the existence of the Ethylene Glycol makes the boundary layer thicker.
5. Ag is more effective among the nanoparticles (Cu, Al₂O₃, TiO₃).

NOMENCLATURE

$\rho_{nf} = (1 - \varphi)\rho_f + \varphi\rho_s$	Density
$(\rho c_p)_{nf} = (1 - \varphi)(\rho c_p)_f + \varphi(\rho c_p)_s$	Heat capacitance
$(\beta)_{nf} = (1 - \varphi)(\beta)_f + \varphi(\beta)_s$	Thermal expansion coefficient
$k_{nf} = k_f \frac{k_s + 2k_f - 2\varphi(k_f - k_s)}{k_s + 2k_f + 2\varphi(k - k_s)}$	Thermal conductivity of the nanofluid
$\alpha_{nf} = \frac{k_{nf}}{(\rho c_p)_{nf}}$	Thermal diffusivity

$\mu_{nf} = \frac{\mu_f}{(1-\phi)^{2.5}}$	Dynamic viscosity	$\rho(kgm^{-3})$	Density of the fluid
$Pr = \frac{\theta_f}{\alpha_f}$	Prandtl number	SUBSCRIPTS	
$C_p (J kg^{-1}K^{-1})$	Specific heat at constant pressure	f	Base fluid
$g(ms^{-2})$	Gravitational acceleration	nf	Base nanofluid
$k(Wm^{-1}K^{-1})$	Thermal conductivity	s	Solid particle
$L(m)$	Base length		
Nu	Nusselt number		
Ri	Richardson number		
Re	Local Reynolds number		
$T(K)$	Dimensional temperature		
$(u, v)(ms^{-1})$	Velocity components, along x, y direction respectively		
(U, V)	Dimensionless velocity components, along X, Y direction respectively		
(x, y)	Cartesian coordinates		
(X, Y)	Non dimensional Cartesian coordinates		
$q_w (Wm^{-2})$	Heat flux		

GREEK SYMBOLS

$\alpha(m^2s^{-1})$	Thermal diffusivity
$\beta(K^{-1})$	Thermal expansion coefficient
ϕ	Solid volume fraction
θ	Non dimensional temperature
$\mu(kgm^{-1}s^{-1})$	Dynamic viscosity of the fluid
$\nu(m^2s^{-1})$	Kinematic viscosity of the fluid

REFERENCES

- [1] Ferdows M, Shamima Islam and Beg OA. Numerical simulation of Marangoni Magneto hydrodynamic Bio-Nanofluid convection from a Non-isothermal surface with Magnetic Induction effects: A Bio-Nanomaterial Manufacturing Transport Model. *Journal of Mechanics in Medicine and Biology* 2014; 14(3): 1-32.
- [2] Hellums JD and Churchill SW. Transient and steady state free and natural convection, numerical solutions: Part 1. The isothermal vertical plate, *AIChE J* 1962; 8: 690-692. <https://doi.org/10.1002/aic.690080525>
- [3] Soundalgekar VM and Ganesan P. Finite difference analysis of transient free convection with mass transfer on an isothermal vertical flat plate. *Int J Eng Sci* 1981; 19: 757-770. [https://doi.org/10.1016/0020-7225\(81\)90109-9](https://doi.org/10.1016/0020-7225(81)90109-9)
- [4] Remeli A, Arifin NM, Nazar R, Ismail F and Pop I. Marangoni-driven Boundary Layer Flow in a Nanofluid with Suction and Injection. *World Applied Sciences Journal* 2012; 17: 21-26.
- [5] Khan WA, Hamad MAA and Ferdows M. Heat transfer analysis for Falkner–Skan boundary layer nanofluid flow past a wedge with convective boundary condition considering temperature-dependent viscosity. *J Nanoeng Nanosyst* 2012; 227(1): 19-27.
- [6] Rossow VJ. On flow of electrically conducting fluid over a flat plate in the presence of a magnetic field. *NACA TR.1358*, 1958.
- [7] Soundalgekar VM, Gupta SK and Aranake RN. Free convection effects on the MHD Stokes problem for a vertical plate. *Nucl Eng Des* 1979; 51: 403-407. [https://doi.org/10.1016/0029-5493\(79\)90127-4](https://doi.org/10.1016/0029-5493(79)90127-4)
- [8] Elbashesy EMA. Heat and Mass transfer along a vertical plate with variable surface tension and concentration in the presence of magnetic field. *Int J Eng Sci* 1997; 34(5): 515-522. [https://doi.org/10.1016/S0020-7225\(96\)00089-4](https://doi.org/10.1016/S0020-7225(96)00089-4)
- [9] Ganesan P and Palani G. Numerical solution of unsteady MHD flow past a semi-infinite isothermal vertical plate, in: *Proceedings of the 6th ISHMT/ASME Heat and Mass Transfer Conference and 17th National Heat and Mass Transfer Conference*, Kalpakkam, India 2004; 5-7: 184-187.
- [10] Aydin O and Kaya A. Radiation effect on MHD mixed convection flow about a permeable vertical plate. *Heat Mass Transfer* 2008; 45: 239-246. <https://doi.org/10.1007/s00231-008-0428-y>
- [11] Khan S, Karim I, Alam MM, Ferdows M and Beg OA. Explicit Numerical study of Unsteady Hydromagnetic Mixed Convective Nanofluid flow from an Exponential Stretching sheet in Porous media. *Appl Nanosci* 2014; 4: 943-957. <https://doi.org/10.1007/s13204-013-0275-0>
- [12] Jhankal AK and Kumar M. MHD Boundary layer flow past a stretching plate with heat transfer. *Int J Eng Sci* 2013; 2(3): 9-13.
- [13] Khan M and Khan WA. MHD boundary layer flow of a power-law nanofluid with new mass flux condition. *AIP Adv* 2016; 6: 025211.

- <https://doi.org/10.1063/1.4942201>
- [14] Putra N, Roetzel W and Das SK. Natural convection of nanofluids. *Heat Mass Transfer* 2003; 39: 775-784.
<https://doi.org/10.1007/s00231-002-0382-z>
- [15] Wen D, Lin G, Vafai S and Zhang K. Review of nanofluids for heat transfer applications. *Particuology* 2009; 7: 141-150.
<https://doi.org/10.1016/j.partic.2009.01.007>
- [16] King, Ki JYT and Choi CK. Analysis of convective instability and heat transfer characteristics of nanofluids. *Phys Fluids* 2004; 16(7): 2395-2401.
<https://doi.org/10.1063/1.1739247>
- [17] Jang SP, Choi SUS. Effects of various parameters on nonfluid thermal conductivity. *J Heat Transfer* 2007; 129: 617-623.
<https://doi.org/10.1115/1.2712475>
- [18] Carnahan B, Luther HA and Wilkes JO. *Applied Numerical Methods*. John Wiley and sons, New York 1969.
- [19] Don Liu, Qin Chen and Yifan W. A Sixth Order Accuracy Solution to a System of Nonlinear Differential Equations with Coupled Compact Method. *J Comp Eng* 2013; 1-10: Article ID 432192.
- [20] Don L, Weijia K and Andrew T. High-order compact implicit difference methods for parabolic equations in Geodynamo simulation. *Adv Math Phys* 2009; 1-23: Article ID 568296.

Received on 05-10-2016

Accepted on 21-11-2016

Published on 31-12-2016

DOI: <http://dx.doi.org/10.15377/2409-9848.2017.04.01.01>

© 2017 Ferdows *et al.*; Avanti Publishers.

This is an open access article licensed under the terms of the Creative Commons Attribution Non-Commercial License (<http://creativecommons.org/licenses/by-nc/3.0/>) which permits unrestricted, non-commercial use, distribution and reproduction in any medium, provided the work is properly cited.